RESEARCH

Evolution of Flame Displacement Speed Within Flame Front in Different Regimes of Premixed Turbulent Combustion

Nilanjan Chakraborty[1] · Cesar Dopazo[2] · Harry Dunn[1] · Umair Ahmed[1]

Abstract

A transport equation for the flame displacement speed evolution in premixed flames is derived from first principles, and the mean behaviours of the terms of this equation are analysed based on a Direct Numerical Simulation database of statistically planar turbulent premixed flames with a range of different Karlovitz numbers. It is found that the regime of combustion (or Karlovitz number) affects the statistical behaviour of the mean contributions of the terms of the displacement speed transport equation which are associated with the normal strain rate and curvature dependence of displacement speed. The contributions arising from molecular diffusion and flame curvature play leading order roles in all combustion regimes, whereas the terms arising from the flame normal straining and reactive scalar gradient become leading order contributors only for the flames with high Karlovitz number values representing the thin reaction zones regime. The mean behaviours of the terms of the displacement speed transport equation indicate that the effects arising from fluid-dynamic normal straining, reactive scalar gradient and flame curvature play key roles in the evolution of displacement speed. The mean characteristics of the various terms of the displacement speed transport equation are explained in detail and their qualitative behaviours can be expounded based on the behaviours of the corresponding terms in the case of 1D steady laminar premixed flames. This implies that the flamelet assumption has the potential to be utilised for the purpose of any future modelling of the unclosed terms of the displacement speed transport equation even in the thin reaction zones regime for moderate values of Karlovitz number.

Keywords Displacement speed · Normal strain rate · Curvature · Premixed flame · Karlovitz number · Direct numerical simulations

1 Introduction

Propagation in the local normal direction of the flame surface plays a pivotal role in premixed turbulent combustion. The speed with which the premixed flame surface moves normal to itself with respect to an initially coincident material surface is commonly referred

---

✉ Nilanjan Chakraborty
nilanjan.chakraborty@newcastle.ac.uk

[1] School of Engineering, Newcastle University, Newcastle-Upon-Tyne NE1 7RU, UK

[2] School of Engineering and Architecture - Fluid Mechanics Area, University of Zaragoza, Zaragoza, Spain

to as the flame displacement speed S_d. The displacement speed S_d statistics play a key role in the level-set and Flame Surface Density (FSD) based modelling approaches of turbulent premixed combustion (Peters 2000; Chakraborty and Cant, 2007a; Han and Huh 2008; Chakraborty and Cant 2009).

It has been demonstrated in several previous analyses that local flame curvature (Peters et al. 1998; Echekki and Chen 1999; Chen and Im, 1998; Chakraborty and Cant 2005, 2006, 2007b; Klein et al. 2006; Chakraborty et al. 2011; Nivarti et al., 2019; Herbert et al. 2020; Ozel-Erol et al. 2021; Chakraborty et al. 2022), strain rate (Chakraborty and Cant 2004, 2006; Klein et al. 2006; Chakraborty et al. 2011; Nivarti et al., 2019; Ozel-Erol et al. 2021) and flame stretch rate (Chen and Im, 1998; Chakraborty et al., 2007b; Chakraborty et al. 2011; Nivarti et al., 2019; Ozel-Erol et al. 2021) have a significant influence on the local flame displacement speed S_d distribution in premixed turbulent flames. The strain rate, curvature and flame stretch rate dependences of flame displacement speed S_d are needed in the level-set (Peters 2000) and Flame Surface Density (FSD) (Chakraborty and Cant, 2007a; Han and Huh 2008; Chakraborty and Cant 2009) based methodologies of turbulent premixed combustion modelling. Although the flame displacement speed can be expressed in terms of reaction rate and diffusion rate imbalance and the reactive scalar gradient (Peters et al. 1998; Echekki and Chen 1999; Chen and Im, 1998; Chakraborty and Cant 2004, 2005, 2006, 2007b; Klein et al. 2006; Chakraborty et al., 2007b;Chakraborty et al. 2011; Nivarti et al., 2019; Herbert et al. 2020; Ozel-Erol et al. 2021; Chakraborty et al. 2022), the physical processes, which determine the evolution of displacement speed within the flame-front, have not been analysed in detail in the existing literature (Yu et al. 2021a, 2021b). Yu and coworkers (Yu et al. 2021a, 2021b) analysed the surface-averaged value of displacement speed (i.e., $\overline{\left(S_d\right)}_s = \overline{S_d|\nabla c|}/\overline{|\nabla c|}$ (Trouvé and Poinsot, 1994; Boger et al., 1998), where the overbar signifies an appropriate averaging operation, and c is the reaction progress variable) for constant density reaction wave (Yu et al. 2021a) and variable density premixed turbulent flames (Yu et al. 2021b) using Direct Numerical Simulations (DNS) data. The surface averaged value of displacement speed $\overline{\left(S_d\right)}_s$ is used for the FSD based closure but the information of the un-weighted displacement speed S_d is also necessary for both the FSD (Chakraborty and Cant, 2007a; Han and Huh 2008; Chakraborty and Cant 2009) and level-set (i.e., $G-$ equation approach) (Peters 2000) based approaches. The governing equation of the level-set (i.e., $G-$ equation) approach involves S_d, which also appears in the kinematic form of the reaction progress variable c transport equation. Moreover, S_d appears explicitly in the transport equation of $|\nabla c|$, which is similar to the flame surface ratio $\sigma = |\nabla G|$ transport equation in the context of level-set approach. This was discussed in detail by Bray and Peters (1994) and thus is not repeated here. In the transport equation of the flame surface ratio $\sigma = |\nabla G|$, the quantities such as displacement speed, flame surface ratio and flame curvature change in space and time. By the same token, the transport equation of S_d can be derived based on the kinematic form of the reaction progress variable transport equation, which can also be used as the governing equation in the level-set approach (Bray and Peters, 1994). It is worth noting that this paper does not deal with the modelling of displacement speed but focuses on the analysis of the statistical behaviours of the different terms of the displacement speed transport equation. The statistical behaviours of the terms in the un-weighted displacement speed transport equation are yet to be analysed in detail for different regimes of premixed turbulent combustion but this analysis is needed for the identification of the physical processes which affect the evolution of displacement speed within the flame front. This aspect is addressed in this paper by deriving a transport equation of flame displacement speed S_d from the first

principle. The mean behaviours of the terms of this transport equation have been analysed using three-dimensional DNS data of statistically planar turbulent premixed flames ranging from the wrinkled/corrugated flamelets regime to the thin reaction zones regime (Ahmed et al. 2019; Brearley et al. 2019; Varma et al. 2021). The main objectives of the present analysis are as follows:

(a)   To demonstrate the mean behaviours of the various terms of the transport equation for flame displacement speed S_d for statistically planar flames ranging from the wrinkled/corrugated flamelets regime to the thin reaction zones regime of premixed turbulent combustion.
(b)   To provide physical explanations for the observed behaviours of the different terms in the S_d transport equation and their variations in response to the changes in Karlovitz number.
(c)   To indicate the implications of the above findings from the point of view of premixed turbulent combustion modelling.

The rest of the paper is organised as follows. The mathematical background and numerical implementation related to the current work are provided in the next two sub-sections. After that results are presented and subsequently discussed. A summary of main findings is provided along with conclusions in the final section of this paper.

2 Mathematical Background

In premixed turbulent combustion, the reactive scalar field is often characterised by a reaction progress variable c. The reaction progress variable c can be defined based on a suitable reactant mass fraction Y_R as: $c = (Y_{R0} - Y_R)/(Y_{R0} - Y_{R\infty})$ where subscripts 0 and ∞ refer to values in unburned gas and fully burned products, respectively. The transport equation of c is given by:

$$\rho[\partial c/\partial t + u_j \partial c/\partial x_j] = \dot{w} + \nabla \bullet (\rho D \nabla c) \tag{1}$$

where ρ, u_j, D and $\dot{w}$ are gas density, j^{th} component of fluid velocity, progress variable diffusivity and reaction rate of progress variable, respectively. Equation 1 can be rewritten in a kinematic form for a given c-isosurface as $d^c c/dt = \left[\partial c/\partial t + V_j \partial c/\partial x_j\right] = 0$ where $V_j = u_j + S_d N_j$ is the jth component of the flame propagation velocity with $\overline{N} = -\nabla c/|\nabla c|$ being the local flame normal vector. According to these definitions, the flame normal points towards the reactants. The kinematic form of the reaction progress variable transport equation can alternatively be written as:

$$\left[\partial c/\partial t + u_j \partial c/\partial x_j\right] = S_d|\nabla c| \tag{2}$$

A comparison between Eqs. 1 and 2 yields the following expression for S_d (Poinsot and Veynante 2001):

$$S_d = [\dot{w} + \nabla \bullet (\rho D \nabla c)]/\rho|\nabla c| \tag{3}$$

Applying isosurface-tracking total derivative d^c/dt to Eq. 3 yields:

$$d^c S_d / dt = (1/|\nabla c|) d^c \left[\dot{w} + \nabla \cdot (\rho D \nabla c) / \rho \right] / dt - \left[\dot{w} + \nabla \cdot (\rho D \nabla c) / \rho |\nabla c|^2 \right] d^c |\nabla c| / dt \tag{4}$$

It has been demonstrated elsewhere (Pope, 1988; Dopazo et al. 2015, 2018) that $d^c |\nabla c| / dt$ can be expressed as:

$$d^c |\nabla c| / dt = -\left(a_N + N_j \partial S_d / \partial x_j \right) |\nabla c| \tag{5}$$

Using Eq. 5 in Eq. 4 yields:

$$\frac{d^c S_d}{dt} = \frac{d^c}{dt} \left[\frac{\dot{w} + \nabla \cdot (\rho D \nabla c)}{\rho |\nabla c|} \right] = \frac{1}{|\nabla c|} \frac{d^c}{dt} \left[\frac{\dot{w} + \nabla \cdot (\rho D \nabla c)}{\rho} \right] + S_d \left(a_N + N_j \frac{\partial S_d}{\partial x_j} \right) \tag{6}$$

For low Mach number globally adiabatic flames with unity Lewis number, the non-dimensional temperature $\theta = (T - T_0)/(T_{ad} - T_0)$ can be equated to the reaction progress variable c, where T_0 and T_{ad} are the unburned gas temperature and adiabatic flame temperature, respectively. Under the assumption of unity Lewis number with low Mach number and globally adiabatic conditions, $\dot{w}/\rho$ becomes a function of c (i.e., $\dot{w}/\rho = f(c)$), which leads to:

$$d^c (\dot{w}/\rho)/dt = f'(c) d^c c/dt = 0 \tag{7}$$

In the non-unity Lewis number case $\dot{w}/\rho$ becomes a function of both c and θ and thus under this condition $d^c (\dot{w}/\rho)/dt$ does not become zero and its exact value depends on the value of Lewis number and the choice of chemical mechanism. The effects of non-unity Lewis number on the terms of the transport equation of S_d are kept beyond the scope of this analysis and will not be considered henceforth in this paper.

Subject to the assumption that the density-weighted diffusivity is constant (i.e., $\rho D = const.$), one gets:

$$\frac{d^c}{dt} \left[\frac{\nabla \cdot (\rho D \nabla c)}{\rho} \right] = \frac{d^c}{dt} \left(D \frac{\partial^2 c}{\partial x_j \partial x_j} \right) = \frac{\partial^2 c}{\partial x_j \partial x_j} \frac{d^c D}{dt} + D \frac{\partial^2}{\partial x_j \partial x_j} \left(\frac{\partial c}{\partial t} \right) + D V_k \frac{\partial^2}{\partial x_j \partial x_j} \left(\frac{\partial c}{\partial x_k} \right) \tag{8}$$

Taking the double derivative of $d^c c / dt = \left[\partial c / \partial t + V_j \partial c / \partial x_j \right] = 0$ provides:

$$\frac{\partial}{\partial t} \left(\frac{\partial^2 c}{\partial x_j \partial x_j} \right) + V_k \frac{\partial}{\partial x_k} \left(\frac{\partial^2 c}{\partial x_j \partial x_j} \right) = 2 \left(\frac{\partial u_k}{\partial x_j} + S_d \frac{\partial N_k}{\partial x_j} + N_k \frac{\partial S_d}{\partial x_j} \right) \frac{\partial}{\partial x_j} \left(N_k |\nabla c| \right) + N_k$$
$$|\nabla c| \left[\frac{\partial^2 u_k}{\partial x_j \partial x_j} + \frac{\partial S_d}{\partial x_j} \frac{\partial N_k}{\partial x_j} + S_d \frac{\partial^2 N_k}{\partial x_j \partial x_j} + \frac{\partial N_k}{\partial x_j} \frac{\partial S_d}{\partial x_j} + N_k \frac{\partial^2 S_d}{\partial x_j \partial x_j} \right] \tag{9}$$

Substituting Eq. 9 in Eq. 8 provides:

$$\frac{d^c}{dt} \left[\frac{\nabla \cdot (\rho D \nabla c)}{\rho} \right] = \left(\frac{\partial^2 c}{\partial x_j \partial x_j} \right) \frac{d^c D}{dt} + D \left[2 \frac{\partial u_k}{\partial x_j} \frac{\partial N_k}{\partial x_j} |\nabla c| + S_d \frac{\partial N_k}{\partial x_j} \frac{\partial N_k}{\partial x_j} |\nabla c| \right.$$
$$\left. + 2 \left(N_k \frac{\partial u_k}{\partial x_j} + \frac{\partial S_d}{\partial x_j} \right) \frac{\partial |\nabla c|}{\partial x_j} + N_k |\nabla c| \frac{\partial^2 u_k}{\partial x_j \partial x_j} + |\nabla c| \frac{\partial^2 S_d}{\partial x_j \partial x_j} \right] \tag{10}$$

Using Eq. 10 in Eq. 4 yields:

$$\frac{\partial S_d}{\partial t} + u_j \frac{\partial S_d}{\partial x_j} = \underbrace{S_d \left(a_N + N_j \frac{\partial S_d}{\partial x_j} \right)}_{T_1} + \underbrace{D \frac{\partial^2 S_d}{\partial x_j \partial x_j}}_{T_2} - \underbrace{N_j S_d \frac{\partial S_d}{\partial x_j}}_{T_3}$$

$$+ \underbrace{D \left(N_k \frac{\partial^2 u_k}{\partial x_j \partial x_j} + S_d \frac{\partial N_k}{\partial x_j} \frac{\partial N_k}{\partial x_j} + 2 \frac{\partial u_k}{\partial x_j} \frac{\partial N_k}{\partial x_j} \right)}_{T_4} + \underbrace{2D \left(N_k \frac{\partial u_k}{\partial x_j} + \frac{\partial S_d}{\partial x_j} \right) \frac{\partial (ln|\nabla c|)}{\partial x_j}}_{T_5} +$$

$$\underbrace{\frac{\partial^2 c}{\partial x_j \partial x_j} \frac{1}{|\nabla c|} \left(\frac{\partial D}{\partial t} + u_j \frac{\partial D}{\partial x_j} + N_j S_d \frac{\partial D}{\partial x_j} \right)}_{T_6} \tag{11}$$

The terms on the left-hand side of Eq. 11 are the transient and advection terms. The term T_1 accounts for the effects of effective normal strain rate (i.e., $a_N^{eff} = N_i N_j \partial u_i / \partial x_j + N_j \partial S_d / \partial x_j$) (Dopazo et al., 2015, 2018) on the flame displacement speed evolution, whereas $T_2 = D\nabla^2 S_d$ represents the molecular diffusion rate of S_d. The term T_1 vanishes in the unstretched laminar planar premixed flame because a_N^{eff} is identically zero under this condition. The term T_3 arises due to the additional normal strain rate arising from flame normal propagation (i.e., $N_j \partial S_d / \partial x_j$) (Dopazo et al., 2015, 2018) and will henceforth be referred to as the propagation term. The terms within T_4 arise due to the correlations between flame normal and velocity gradients (representing the first and third sub-terms of T_4) and the correlation between displacement speed and flame curvature tensor components (representing the second sub-term of T_4). The term T_5 arises due to the involvement of $\partial (ln|\nabla c|)/\partial x_j$ and the correlation between flame normal components with the propagation velocity gradient (i.e., $N_k \partial V_k / \partial x_j = N_k \partial u_k / \partial x_j + \partial S_d / \partial x_j$). The flame is stationary (i.e., $V_k = 0$) for a steady state unstretched laminar premixed flame and thus, this term vanishes under this condition. The term T_6 originates due to mass diffusivity variation because all the terms involve either temporal (see the first sub-term of T_6) or spatial gradient of diffusivity (see second and third sub-terms of T_6).

It is worth noting that $\overline{(S_d)}_s = \overline{S_d |\nabla c|} / \overline{|\nabla c|}$ depends on the correlation between S_d and $|\nabla c|$. Thus, the transport equation of $\overline{(S_d)}_s$ is different from the transport equation of the un-weighted displacement speed S_d as some additional terms appear in the transport equation of $\overline{(S_d)}_s$. Interested readers are referred to Yu et al. (2021a, b) for the transport equation of $\overline{(S_d)}_s$. The transport equation of $\overline{(S_d)}_s$ can be derived using chain rule using Eqs. 5 and 11. The present analysis will henceforth focus on the transport equation of S_d (i.e., Eq. 11) and the mean behaviours of T_1, T_2, T_3, T_4, T_5 and T_6 will be discussed in detail in the Results section of this paper.

3 Numerical Implementation

The statistical behaviours of T_1, T_2, T_3, T_4, T_5 and T_6 have been analysed using DNS simulations of statistically planar premixed flames. These simulations have been conducted using a well-known code SENGA + (Jenkins and Cant, 1999; Chakraborty and Cant 2005, 2006, 2007b; Klein et al. 2006; Chakraborty et al. 2011; Nivarti et al., 2019; Herbert et al. 2020; Ozel-Erol et al. 2021; Chakraborty et al. 2022). In SENGA +, all first and second-order derivatives for the internal grid points are evaluated using a 10th-order central difference

scheme but the order of accuracy gradually drops to a one-sided 2nd-order scheme at the non-periodic boundaries (Jenkins and Cant, 1999; Chakraborty and Cant 2005, 2006, 2007b; Klein et al. 2006; Chakraborty et al. 2011; Herbert et al. 2020; Ozel-Erol et al. 2021; Chakraborty et al. 2022). An explicit 3rd order low storage Runge–Kutta scheme (Wray 1990) is used for time advancement. The simulation domain has inlet and outlet boundaries in the direction of mean flame propagation (i.e., x−direction), whereas transverse boundaries are taken to be periodic. The outflow boundary is taken to be partially non-reflecting and specified using the Navier–Stokes Characteristic Boundary Conditions (NSCBC) technique (Poinsot and Lele 1992). The mean inlet velocity U_{mean} at the inlet boundary is gradually altered to match the turbulent burning velocity so that the flame remains stationary in the statistical sense within the computational domain. A pseudo-spectral method (Rogallo 1981) is used for the initialisation of the fluctuating velocity field by utilising a homogeneous isotropic incompressible distribution following the Batchelor-Townsend spectrum (Batchelor and Townsend, 1948) for prescribed values of root-mean-square turbulent velocity u' and the integral length scale of turbulence l. The scalar field is initialised by a steady unstretched laminar flame solution. The turbulence in the unburned gas is forced using a modified bandwidth forcing (Klein et al. 2017) in physical space with a forcing term proportional to $(1 - c)$, which maintains both the required values of root-mean-square velocity u' and the integral length scale of turbulence l in the unburned gas. The simulation domain size, the uniform Cartesian grid for discretisation along with the inlet values of root-mean-square turbulent velocity fluctuation normalised by the unstrained laminar burning velocity u'/S_L, integral length scale to the Zel'dovich flame thickness ratio l/δ_z, Damköhler number $Da = lS_L/u'\delta_z$, Karlovitz number $Ka = \left(u'/S_L\right)^{3/2}\left(l/\delta_z\right)^{-1/2}$ and heat release parameter $\tau = (T_{ad} - T_0)/T_0$ are listed in Table 1 where the Zel'dovich flame thickness δ_z is defined as: $\delta_z = \alpha_{T0}/S_L$ with α_{T0} and S_L being the thermal diffusivity and unstrained laminar burning velocity, respectively. The locations of these cases on the Borghi-Peters diagram are shown in Fig. 1 and also mentioned in Table 1, which indicate that the cases considered here span from the wrinkled flamelet regime to the high Karlovitz number thin reaction zones regime. The grid spacing used here ensures at least 10 grid points within $\delta_{th} = (T_{ad} - T_0)/\max|\nabla T|_L$ where T, T_0 and T_{ad} are the dimensional temperature, unburned gas temperature and the adiabatic flame temperature, respectively. The Kolmogorov length scale η is well-resolved with 1.5–2.0 grid points for the simulation parameters considered here.

The chemical mechanism is simplified in the current analysis by a single-step Arrhenius mechanism representing stoichiometric methane-air flame in this analysis in the interests of computational economy allowing for a detailed parametric analysis. The Lewis number of all the species is taken to be unity and the gaseous mixture is taken to be perfect gases. Standard values are taken for Prandtl number (i.e., $Pr = 0.7$), Zel'dovich number

**Table 1** Simulation parameters for all cases considered in this analysis

	u'/S_L	l/δ_z	Da	Ka	τ	Domain size	Grid size
Case—A	1.0	5.25	5.25	0.44	4.5	$140.7\,\delta_z \times (70.35\,\delta_z)^2$	$800 \times (400)^2$
Case—B	3.0	5.25	1.75	2.	4.5	$140.7\,\delta_z \times. (70.35\,\delta_z)^2$	$800 \times (400)^2$
Case – C	5.0	5.25	1.05	4.88	4.5	$140.7\,\delta_z \times (70.35\,\delta_z)^2$	$800 \times (400)^2$
Case – D	7.5	5.25	0.7	8.96	4.5	$140.7\,\delta_z \times (70.35\,\delta_z)^2$	$800 \times (400)^2$
Case—E	10.0	5.25	0.525	13.80	4.5	$140.7\,\delta_z \times (70.35\,\delta_z)^2$	$800 \times (400)^2$

(i.e., $\beta = T_{ac}(T_{ad} - T_0)/T_{ad}^2 = 6.0$ where T_{ac} is the activation temperature), ratio of specific heats (i.e., $\gamma = 1.4$) and the density-weighted diffusivity ρD is taken to be constant for the sake of simplicity. It was demonstrated by Keil et al., (2021a, b) that the flame displacement speed statistics obtained from simple chemistry DNS of stoichiometric methane-air premixed flames remain in good qualitative agreement with the corresponding detailed chemistry simulations (Keil et al. 2021a, b) within the Karlovitz number range considered here. The quantitative differences in flame displacement speed statistics between simple and detailed chemistry DNS for the Karlovitz number range considered here remain comparable to the uncertainties associated with the different definitions of reaction progress variable in detailed chemistry simulations (Keil et al. 2021b). All the cases listed in Table 1 have been simulated until the desired values of both turbulent kinetic energy and integral length scale have been obtained and also the turbulent burning velocity S_T and flame surface area A_T attain statistically stationary states. The simulation times for all cases remain greater than the through-pass time (i.e., $t_{sim} > L_x/U_{mean}$) and are equal to at least 10 eddy turnover times (i.e., $t_{sim} > 10l/u'$).

The distributions of c in the $x - y$ midplane for cases A–E are shown in Fig. 2a–e, respectively. The appearance of isolated pockets of unburned gas within the burned gas region in 2D planes shown in Fig. 2 originates due to intersection of flame wrinkles with the plane but they are not truly unburned gas pockets. This can be verified from the isosurfaces of c isosurfaces, which are shown elsewhere (Ahmed et al. 2019; Varma et al. 2021) and thus are not repeated here. Figure 2a–e show that c-isosurfaces are parallel to each other in case A where the flame shows wrinkling due to large-scale turbulent motion, as expected in the wrinkled/corrugated flamelets regime. However, the preheat zone in cases B–E is affected by the small-scale turbulent eddies, which is reflected in the local occurrences of flame thickening in accordance with the expectations for the thin reaction zones regime combustion (Peters 2000). The scale separation between δ_{th} and η increases with increasing Karlovitz number Ka and thus the localised flame thickening is not significantly evident in case B, but this aspect can be seen from Fig. 2c–e for cases C–E. As the flame structure is affected by the regime of combustion, it can be expected that the evolution of the flame displacement speed is going to be affected by the regime of combustion (i.e., with Ka).

Fig. 1 The cases considered here on the regime diagram
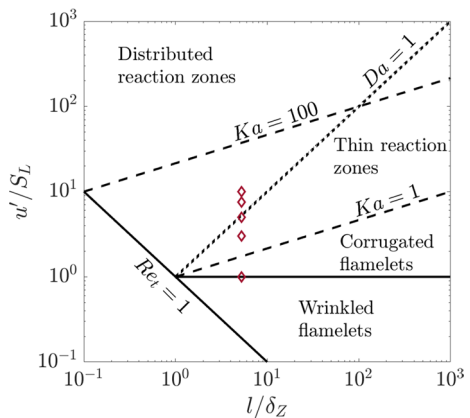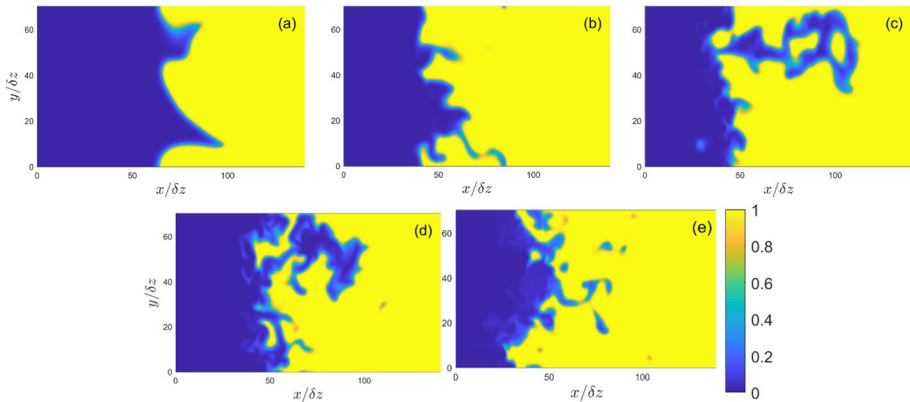
**Fig. 2** Distributions of c in the central $x - y$ midplane for cases (**a–e**) A–E

4 Results and Discussion

The profiles of mean values of S_d/S_L conditioned upon c for cases A–E are shown in Fig. 3, which shows that the mean value of S_d/S_L increases from the unburned to the burned gas side of the flame front as a result of density change due to thermal expansion. It is worth noting that $|\nabla c|$ assumes vanishingly small values for both $c = 0.0$ and 1.0, and thus to avoid numerical uncertainties the data in the range $0.95 > c > 0.05$ is only shown in Fig. 3 and subsequent figures. The mean values of S_d/S_L for cases A-E remain comparable and the differences between cases remain smaller than their standard deviations (not shown here). The mean value of S_d/S_L conditioned upon c remains close to $(1 + \tau c)$ for all cases but the standard deviation of S_d/S_L increases from cases A to E (not shown). Thus, it is worthwhile to consider whether all the terms of the displacement speed transport equation (i.e., Eq. 11) behave similarly in different combustion regimes.

The profiles of the normalised mean values of the terms on the right-hand side of Eq. 11 conditioned upon c are shown in Fig. 4a–e for cases A-E, respectively. It can be seen from Fig. 4a–e that the behaviours of the variations of the mean values of $\{T_1, T_2, T_3, T_4, T_5, T_6\} \times \alpha_{T0}/S_L^3$ change from one case to another. The profiles of the normalised mean values of the total contributions of left and right-hand sides of Eq. 11 conditioned upon c for cases A-E are shown in the Appendix, which shows an excellent agreement between both sides of this equation was obtained. In all cases the magnitude of T_6 remains vanishingly small in comparison to the magnitudes of T_2, T_3 and T_4, which act as leading order contributors to the displacement speed evolution within the flame front. It can be seen from Fig. 4a–e that the magnitudes of T_1 and T_5 remain small in comparison to T_2, T_3 and T_4 in case A but T_1 and T_5 assume comparable magnitudes as those of T_2, T_3 and T_4 in cases B-E. For all cases T_2 assumes positive mean values towards the unburned gas side before becoming negative for $c > 0.7$. The mean value of T_3 reaches the maximum value at around $c = 0.7$, but in cases A and B, the mean values of T_3 assume positive values, whereas the mean values of T_3 in cases D and E remain negative throughout the flame front. The mean value of T_3 assumes negative values towards the unburned gas side but becomes positive towards the burned gas side for cases B and C. The mean value of T_4 remains positive throughout the flame for cases B-E but in case A it assumes negative values for $0.4 < c < 0.6$, whereas just a dip in the mean positive value of T_4 is observed in

Fig. 3 Profiles of mean values of S_d/S_L conditioned upon c for cases A–E
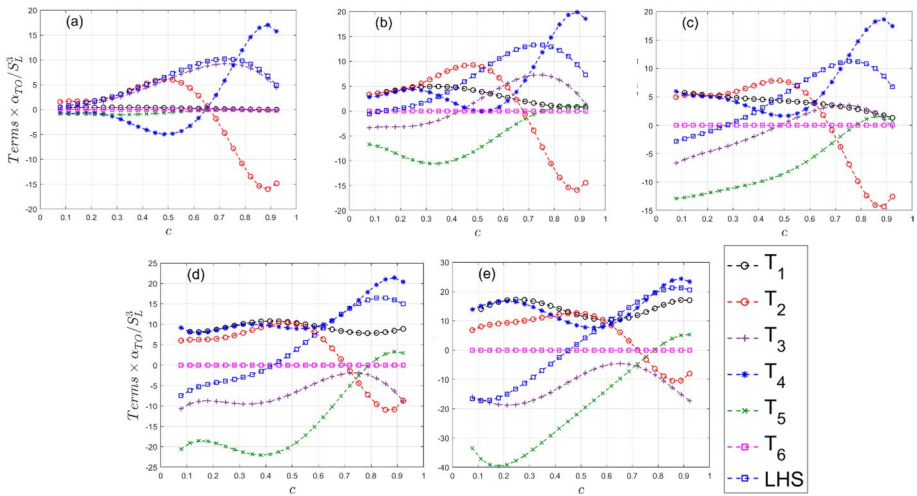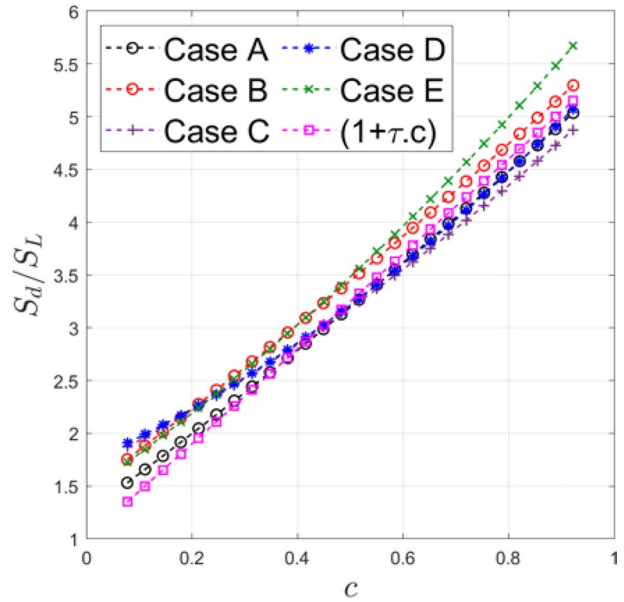

Fig. 4 Profiles of the normalised mean values of $\{T_1, T_2, T_3, T_4, T_5, T_6\}$ and LHS of Eq. 11 conditioned upon c for cases (**a–e**) A–E

cases B-E. The term T_5 assumes negative values for a major part of the flame but becomes weakly positive towards the burned gas side for all cases considered here.

To understand the observed behaviours of the terms shown in Fig. 4a–e, it is worthwhile to consider the variations of the mean values of the components of individual terms in Eq. 11. The profiles of the mean values of the components of T_1 given by $T_1^{(i)} = S_d a_N$ and $T_1^{(ii)} = S_d N_j \partial S_d/\partial x_j$ conditioned upon c for cases A-E are shown in Fig. 5a–e,

respectively. The terms $T_1^{(i)}$ and $T_1^{(ii)}$ assume positive and negative mean values and they almost cancel each other in case A. The likelihood of positive values of $T_1^{(i)}$ decreases from case B-E, which is reflected in the decrease in the range of reaction progress variable for which positive mean values of $T_1^{(i)}$ are obtained. Moreover, the magnitude of negative mean values of $T_1^{(i)}$ towards both unburned and burned gas sides of the flame front increases from case B to case E. The normal strain rate a_N can alternatively be expressed as: $a_N = (e_\alpha \cos^2\theta_\alpha + e_\beta \cos^2\theta_\beta + e_\gamma \cos^2\theta_\gamma)$ where e_α, e_β and e_γ are the most extensive principal strain rate, intermediate principal strain rate and the most compressive principal strain rate, respectively and θ_i is the angle between ∇c and the eigenvector associated with e_i (where $i = \alpha, \beta$ and γ). It has been discussed elsewhere (Chakraborty and Swaminathan 2007; Chakraborty et al. 2009) that ∇c in turbulent premixed flames preferentially collinearly aligns with the eigenvector associated with e_α (i.e., $|\cos\theta_\alpha| \approx 1.0$) when the strain rate induced by flame normal acceleration overwhelms turbulent straining, which is realised for $\tau Da > 1.0$ (Chakraborty and Swaminathan 2007; Chakraborty et al. 2009). By contrast, for $\tau Da < 1.0$, the reactive scalar gradient ∇c in turbulent premixed flames preferentially collinearly aligns with the eigenvector associated with e_γ (i.e., $|\cos\theta_\gamma| \approx 1.0$) as a result of turbulent strain rate dominating over the strain rate induced by flame normal acceleration (Chakraborty and Swaminathan 2007; Chakraborty et al. 2009). However, even for these cases, a collinear alignment of ∇c with the eigenvector associated with e_α can be obtained in the region of intense heat release within the flame. As the eigenvectors are mutually perpendicular to each other, a preferential alignment of ∇c with the eigenvector associated with e_α gives rise to a positive value of $T_1^{(i)}$ in case A. However, the extent of alignment of ∇c with the eigenvector associated with e_γ (e_α) increases (decreases) from case A to case E with a decrease in Da. Moreover, the alignment of ∇c with the eigenvector associated with e_γ is particularly strong on both unburned and burned gas sides of the flame where the heat release effects are weak and thus $T_1^{(i)}$ assumes negative values in these regions in cases B-E with the magnitude of the negative values increasing from case B to case E. However, positive mean–values of $T_1^{(i)}$ are obtained for $0.5 < c < 0.8$ where thermal expansion effects are strong in cases B–E.
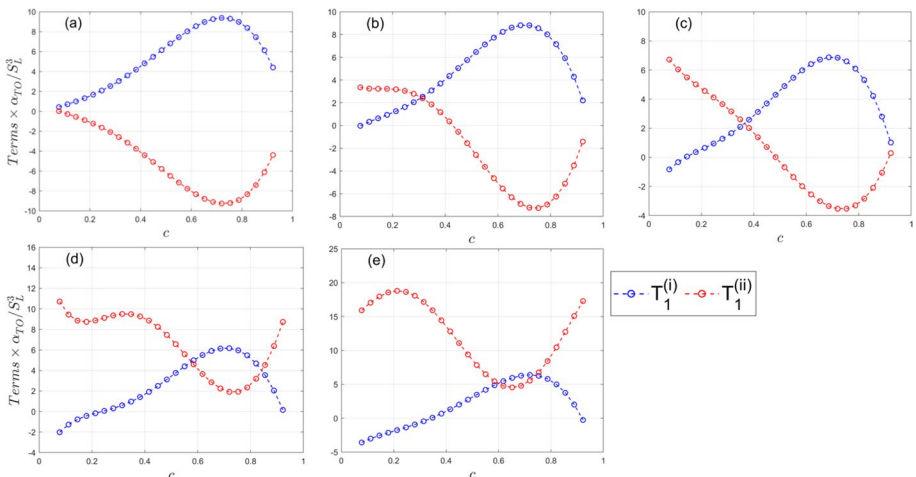
Fig. 5 Profiles of $\{T_1^{(i)}$ and $T_1^{(ii)}\} \times \alpha_{T0}/S_L^3$ conditioned upon c for cases (**a–e**) A–E

In order to explain the mean behaviour of $T_1^{(ii)}$, it is worthwhile to consider the components of $S_d = (S_r + S_n) - 2D\kappa_m$ (Peters et al. 1998; Echekki and Chen 1999) where $S_r = \dot{w}/\rho|\nabla c|$ and $S_n = \vec{N} \cdot \nabla(\rho D \vec{N} \cdot \nabla c)/\rho|\nabla c|$ are the reaction and normal diffusion components of displacement speed, respectively (Peters et al. 1998; Echekki and Chen 1999) and $\kappa_m = 0.5 \partial N_i/\partial x_i$ is the flame curvature which is positive (negative) when the flame is convex (concave) towards the reactants. This suggests that the mean values of S_d for statistically planar flames remain close to the mean values $(S_r + S_n)$ because the mean contribution of $(-2D\kappa_m)$ remain negligible. This was demonstrated elsewhere (Chakraborty and Cant 2004, 2005) and a similar behaviour was found in this database. The mean value of $(S_r + S_n)$ increases with increasing c, which leads to the negative mean value of $N_j \partial(S_r + S_n)/\partial x_j$. However, $-2N_j(\partial D\kappa_m)/\partial x_j$ assumes positive mean values due to the increase in D with increasing c. The contribution of $(-2D\kappa_m)$ to S_d remains weak for small values of Ka but this contribution strengthens with increasing Ka, which is consistent with the scaling arguments by Peters (2000). Thus, $N_j \partial(S_r + S_n)/\partial x_j$ remains the major contribution for small values of Ka, whereas the mean contribution of $-2N_j(\partial D\kappa_m)/\partial x_j$ becomes important for high Ka flames. Therefore, the mean value of $T_1^{(ii)}$ remains mostly negative for cases A and B, whereas the mean value of $T_1^{(ii)}$ remains mostly positive for cases D and E and the mean value of $T_1^{(ii)}$ assumes positive (negative) values towards the unburned (burned) gas side of the flame in case C. A comparison between the expressions of $T_1^{(ii)}$ and T_3 from Eq. 11 reveals $T_3 = -T_1^{(ii)}$ and thus the variation of the mean values of T_3 with c is opposite to that of $T_1^{(ii)}$. The term T_3 and $T_1^{(ii)}$ are retained in Eq. 11 in order to indicate the origin of the terms in the displacement speed transport equation.

For low-Mach number, unity Lewis number globally adiabatic premixed flames, the displacement speed S_d can be expressed as: (Chakraborty and Cant 2004, 2005):

$$S_d = (\partial u_j/\partial x_j)(1 + \tau c)/\tau|\nabla c| \tag{12}$$

As the dilatation rate $(\partial u_j/\partial x_j)$ scales as: $(\partial u_j/\partial x_j) \sim \tau S_L|\nabla c|$ (Chakraborty and Cant 2004, 2005), $\partial^2 S_d/\partial x_j \partial x_j$ can be scaled as $\partial^2 S_d/\partial x_j \partial x_j \sim \tau S_L \partial^2 c/\partial x_j \partial x_j$. The term $\partial^2 c/\partial x_j \partial x_j$ assumes positive (negative) mean values towards the unburned (burned) gas side of the flame front (Chakraborty and Cant 2004, 2005) and thus the mean value of T_2 exhibits positive (negative) values on the unburned (burned) gas side.

The distributions of $\dot{w}$ and $\nabla \cdot (\rho D \nabla c)$ for the different values of c for the steady-state unstretched laminar flame for the present thermochemistry are shown in Fig. 6 for the purpose of supporting the arguments made above regarding the variations of $\nabla^2 c$ (and also for other quantities, which will be discussed later). It can be seen that $\dot{w}$ in the steady state laminar flame assumes a non-negligible value for $c > 0.5$ and assumes a peak value around $c = 0.8$. By contrast, $\nabla \cdot (\rho D \nabla c)$ takes positive values towards the unburned gas before assuming negative values towards the burned gas side. As ρD is assumed to be constant for this database, the variation of $\nabla \cdot (\rho D \nabla c)$ shown in Fig. 6 originates due to $\nabla^2 c$. This behaviour is qualitatively similar to previous DNS results for turbulent premixed flames (Chakraborty and Cant 2004, 2005). This suggests that $\partial^2 S_d/\partial x_j \partial x_j \sim \tau S_L \partial^2 c/\partial x_j \partial x_j$ is expected to assume positive (negative) mean values towards the unburned (burned) gas side of the flame front. It can be seen from Fig. 6 that $\dot{w} + \nabla \cdot (\rho D \nabla c) = \rho S_d|\nabla c|$ remains identical to $\rho_0 S_L|\nabla c|$ for the unstretched 1D laminar premixed flame and the maximum value of $\rho_0 S_L|\nabla c|$ is obtained around $c \approx 0.7$. This suggests that $N_j \partial|\nabla c|/\partial x_j$ in the 1D unstretched laminar premixed flame assumes negative value towards the unburned gas side but it becomes positive towards

Fig. 6 Profiles of $\{\dot{w}, \nabla \cdot (\rho D \nabla c), \dot{w} + \nabla \cdot (\rho D \nabla c), \{\rho_0 S_L |\nabla c|\} \times \alpha_{T0}/\rho_0 S_L^2$ conditioned upon c for 1D steady state unstretched laminar premixed flame
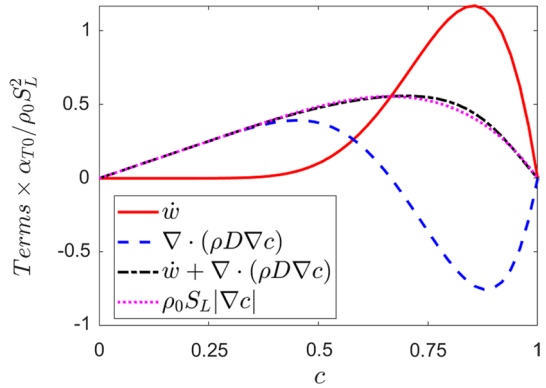

the burned gas side of the flame front. This will be utilised to explain the mean behaviours of T_4 and T_5 in turbulent flames, which will be discussed next in the paper.

The profiles of mean values of the components of T_4 (i.e., $T_4^{(i)} = DN_k \partial^2 u_k / \partial x_j \partial x_j$, $T_4^{(ii)} = DS_d (\partial N_k / \partial x_j)(\partial N_k / \partial x_j)$ and $T_4^{(iii)} = 2D(\partial u_k / \partial x_j)(\partial N_k / \partial x_j))$ conditioned upon c for cases A–E are shown in Fig. 7a–e, respectively. Figure 7a–e show that the mean values of $T_4^{(i)}$ remain the major contributor to the mean value of T_4 for all cases. The term $(\partial N_k / \partial x_j)(\partial N_k / \partial x_j)$ can be expressed as:

$$(\partial N_k / \partial x_j)(\partial N_k / \partial x_j) = 4\kappa_m^2 + (N_{1,2}^2 + N_{2,1}^2 - 2N_{1,1}N_{2,2}) + (N_{1,3}^2 + N_{3,1}^2 - 2N_{1,1}N_{3,3}) + (N_{2,3}^2 + N_{3,2}^2 - 2N_{2,2}N_{3,3}) \tag{13}$$

where $N_{i,j}$ refers to $(\partial N_i / \partial x_j)$. The above expression indicates that the net contribution of the 2nd to 4th terms on the right-hand side of Eq. 13 is likely to be small. Thus, the behaviour of $T_4^{(ii)}$ is principally dictated by $4DS_d \kappa_m^2 = 4D(S_r + S_n)\kappa_m^2 - 8D^2\kappa_m^3$. For statistically planar flames κ_m exhibits mostly symmetric distribution around the zero-mean value (Chakraborty and Cant 2004, 2005) and thus the mean contribution of $(-8D^2\kappa_m^3)$ remains negligible in comparison to the mean contribution of $4D(S_r + S_n)\kappa_m^2$, which scales as $4D(S_r + S_n)\kappa_m^2 \sim 4D\rho_0 S_L \kappa_m^2/\rho$. The range of curvature values (or the width of curvature probability density function) increases with increasing flame wrinkling with an increase in u'/S_L and thus the mean contribution of $T_4^{(ii)}$ remains positive but the magnitude of the mean value of $T_4^{(ii)}$ increases from case A to case E. To explain the behaviours of $T_4^{(i)}$ and $T_4^{(iii)}$, it is worthwhile to consider a steady laminar flame condition, especially for the cases, which represent the flamelet regime of combustion. For a steady-state unstretched laminar flame condition, one gets $u_k = -S_d N_k$, which leads to: $T_4^{(i)} = -T_2 + T_4^{(ii)}$ and $T_4^{(iii)} = -T_4^{(ii)}$. It can indeed be seen from Fig. 7a that the positive mean value of $T_4^{(ii)}$ is cancelled by $T_4^{(iii)}$. Although this is not maintained in cases B-E, the mean value of $T_4^{(iii)}$ remains negative in constrast to positive mean values of $T_4^{(ii)}$ throughout the flame front. The mean behaviour of $T_4^{(i)}$ is mostly qualitatively opposite to that of T_2 but the positive mean contribution of $T_4^{(ii)}$ tends to reduce the negative mean value of $T_4^{(i)}$. The large magnitudes of mean values of T_2 make the mean value of $T_4^{(i)}$ as the major contributor of the mean value of T_4 in all cases considered here.
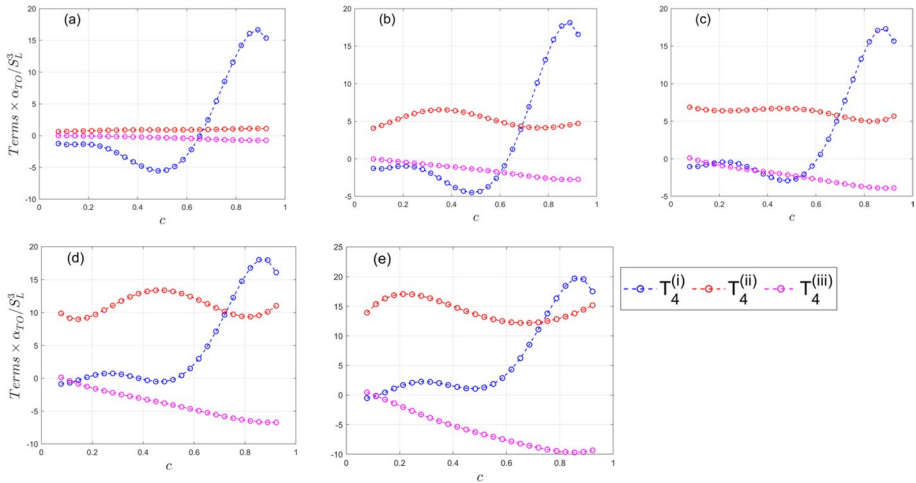
Fig. 7 Profiles of $\{T_4^{(i)}, T_4^{(ii)}$ and $T_4^{(iii)}\} \times \alpha_{T0}/S_L^3$ conditioned upon c for cases (**a**–**e**) A–E

The profiles of mean values of the components of T_5 (i.e., $T_5^{(i)} = 2DN_k(\partial u_k/\partial x_j)(\partial ln|\nabla c|/\partial x_j)$ and $T_5^{(ii)} = 2D(\partial S_d/\partial x_j)(\partial ln|\nabla c|/\partial x_j))$ conditioned upon c for cases A-E are shown in Fig. 8a–e, respectively. It can be seen from Fig. 8a–e that the variations of the mean values of $T_5^{(i)}$ and $T_5^{(ii)}$ are opposite to each other and thus, T_5 does not play a leading role in the transport of S_d in case A where $T_5^{(i)}$ and $T_5^{(ii)}$ cancel each other. In the steady laminar flame, one gets: $T_5^{(i)} = -2D(\partial S_d/\partial x_j)(\partial|\nabla c|/\partial x_j)(1/|\nabla c|) = -T_5^{(ii)}$ and positive (negative) values of $T_5^{(ii)}$ towards the unburned (burned) gas side of the flame-front with a transition from the positive to the negative value where the peak value of $|\nabla c|$ is obtained (i.e. $c \approx 0.7$ for the present thermochemistry). This suggests that negative (positive) values of $T_5^{(i)}$. towards the unburned (burned) gas side of the flame front. The qualitative behaviour of the mean values of $T_5^{(i)}$ and $T_5^{(ii)}$ in turbulent flames are found to be similar to the corresponding variations in the steady unstretched laminar flame case.
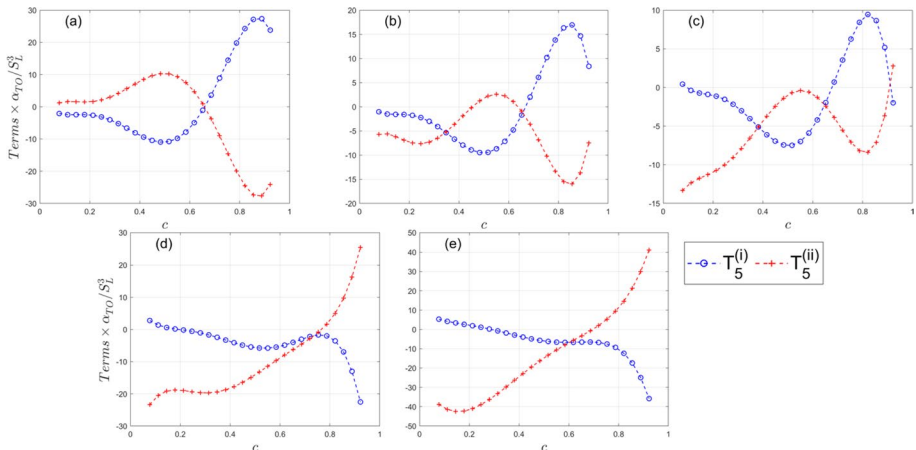
Fig. 8 Profiles of $\{T_5^{(i)}$ and $T_5^{(ii)}\} \times \alpha_{T0}/S_L^3$ conditioned upon c for cases (**a**–**e**) A–E

Subject to the assumption of $\rho D = constant$, $T_6^{(i)}$ can be expressed as: $T_6^{(i)} = D\nabla^2 c(\partial u_j/\partial x_j)/|\nabla c|$. and $T_6^{(ii)} = -D\nabla^2 c(\partial u_j/\partial x_j)/|\nabla c|$. This suggests that $T_6^{(i)}$ and $T_6^{(ii)}$ are expected to cancel each other in all cases. It is worth noting that the mean contribution of T_6 may not be zero when $\rho D \neq constant$ but this term is not expected to play a leading role in the displacement speed transport.

The foregoing discussion suggests that the gradient-based or two-point statistics related to fluid-dynamic normal straining, reactive scalar gradient and flame curvature are expected to play pivotal roles in the evolution of flame displacement speed statistics, which is qualitatively consistent with a recent study that employed Lagrangian tracking to analyse the displacement speed statistics along the trajectory of a fluid parcel (Dave and Chaudhuri 2020). This is in turn reflected in the appreciable correlations of displacement speed with fluid-dynamic strain rates and flame curvature, which have been reported widely in the existing literature (Peters et al. 1998; Echekki and Chen 1999; Chen and Im, 1998; Chakraborty and Cant 2004, 2005, 2006, 2007b; Klein et al. 2006; Chakraborty et al., 2007b; Chakraborty et al. 2011; Nivarti et al., 2019; Herbert et al. 2020; Ozel-Erol et al. 2021; Chakraborty et al. 2022). Furthermore, the qualitative behaviours of T_2, T_4 and T_5 are found to be qualitatively similar to the expected behaviours in the case of 1D steady unstretched laminar premixed flame. However, the qualitative behaviour of the relative importance of the displacement speed transport equation terms, which are associated with the normal strain rate and curvature dependence of displacement speed, change with the variations in Damköhler and Karlovitz numbers (i.e., regime of combustion). This behaviour originates due to the change in the (a) relative alignment of ∇c with strain rate eigenvectors and (b) the strength of the correlation between displacement speed and curvature with the variation of Da. and Ka. It is also worth noting that these changes with the regime of combustion are routinely considered in the flamelet modelling framework (e.g. Peters 2000; Chakraborty and Cant, 2007a; Chakraborty and Cant 2009; Chakraborty and Swaminathan 2007; Chakraborty et al. 2009). Thus, the flamelet assumption has the potential to be applied for the modelling of the terms of the displacement speed transport equation terms for moderate values of Karlovitz number provided the modifications of the (i) relative alignment of ∇c with strain rate eigenvectors and (ii) the strength of the correlation between displacement speed and curvature with the variation of Da. and Ka. are appropriately accounted for.

5 Conclusions

A transport equation of flame displacement speed has been derived based on the first principle subject to some usual assumptions related to thermochemistry and molecular transport. The mean behaviour of the terms of the flame displacement speed transport equation has been analysed based on a DNS database of statistically planar turbulent premixed flames ranging from the wrinkled/corrugated flamelets regime to the thin reaction zones regime with moderate values of Karlovitz number. It has been found that the qualitative behaviour and/or the relative importance of the terms of the displacement speed transport equation, which are associated with the normal strain rate and curvature dependence of displacement speed, change with the variations of Damköhler and Karlovitz numbers. The contributions arising from molecular diffusion and flame curvature act as leading order terms in all combustion regimes, and the contributions of flame normal straining and reactive scalar gradient do not play a significant role for

the flames belonging to the wrinkled/corrugated flamelets regime, but these terms become leading order contributor for the flames representing the thin reaction zones regime. The findings of the current analysis suggest that the gradient-based or two-point statistics-based effects arising from fluid-dynamic normal straining, reactive scalar gradient and flame curvature play pivotal roles in the evolution of flame displacement speed.

The present analysis has been conducted in the context of simple chemistry and unity Lewis number as a starting point for the analysis of the displacement speed transport equation. Thus, further analyses in the presence of detailed chemistry and transport will be needed for a deeper understanding and further insights into differential diffusion effects (e.g., non-unity Lewis number effects) on the displacement speed evolution. This will be the platform for further investigation in this regard.

Appendix

The profiles of the normalised mean values of $(\partial S_d/\partial t + u_j \partial S_d/\partial x_j) \times \alpha_{T0}/S_L^3$ and $\{T_1 + T_2 + T_3 + T_4 + T_5 + T_6\} \times \alpha_{T0}/S_L^3$ conditioned upon c are shown in Fig. 9a–e for cases A–E, respectively. The y-range for the plots in Fig. 9a–e are kept the same as that of Fig. 4a–e for the sake of comparison. It can be seen from Fig. 9a–e that the good agreement (i.e., maximum error of 2%) between LHS and RHS of Eq. 11 has been achieved for all cases considered here.
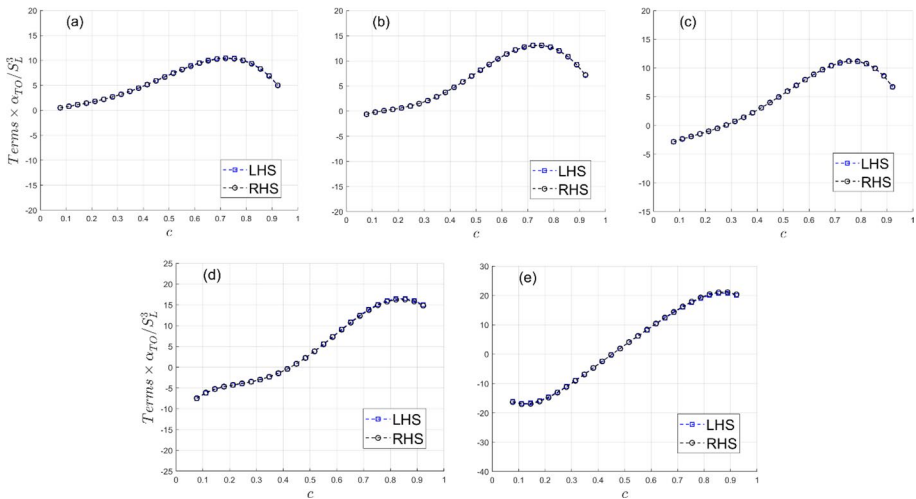
Fig. 9 Profiles of the normalised mean values of $(\partial S_d/\partial t + u_j \partial S_d/\partial x_j) \times \alpha_{T0}/S_L^3$ (LHS) and $\{T_1 + T_2 + T_3 + T_4 + T_5 + T_6\} \times \alpha_{T0}/S_L^3$ (RHS) conditioned upon c for cases (**a**–**e**) A–E

Declarations

Conflict of interest The authors declare that they have no conflict of interest.

Ethical Approval No specific ethical approval is required for this work.

Informed Consent Not applicable for this work.

References

Ahmed, U., Chakraborty, N., Klein, M.: Insights into the bending effect in premixed turbulent combustion using the flame surface density transport. Comb. Sci. Tech. **191**, 898–920 (2019)

Batchelor, G.K., Townsend, A.A.: Decay of turbulence in the final period. Proc. Royal Soc. London Ser. A Math. Phys. Sci. **194**(1039), 527–543 (1948)

Bray, K., Peters, N.: Laminar flamelets in turbulent flames. PA Libby and FA Williams (Academic Press, London), pp. 63-113. (1994)

Brearley, P., Ahmed, U., Chakraborty, N., Lipatnikov, A.N.: Statistical behaviours of conditioned two-point second-order structure functions in turbulent premixed flames in different combustion regimes. Phys. Fluids **31**, 115109 (2019)

Chakraborty, N., Cant, S.: Unsteady effects of strain rate and curvature on turbulent premixed flames in an inlet-outlet configuration. Comb. Flame **137**, 129–147 (2004)

Chakraborty, N., Cant, R.S.: Influence of Lewis number on curvature effects in turbulent premixed flame propagation in the thin reaction zones regime. Phys. Fluids **17**, 105105 (2005)

Chakraborty, N., Cant, R.S.: Influence of Lewis number on strain rate effects in turbulent premixed flame propagation in the thin reaction zones regime. Int. J. Heat Mass Trans. **49**, 2158–2172 (2006)

Chakraborty, N., Cant, R.S.: A-priori analysis of the curvature and propagation terms of the flame surface density transport equation for large eddy simulation. Phys. Fluids **19**, 105101 (2007)

Chakraborty, N., Cant, R.S.: Direct numerical simulation analysis of the flame surface density transport equation in the context of large eddy simulation. Proc. Comb. Inst. **32**, 1445–1453 (2009)

Chakraborty, N., Swaminathan, N.: Influence of Damköhler number on turbulence-scalar interaction in premixed flames, part i: physical insight. Phys. Fluids **19**, 045103 (2007)

Chakraborty, N., Klein, M., Cant, R.S.: Stretch rate effects on displacement speed in turbulent premixed flame kernels in the thin reaction zones regime. Proc. Comb. Inst. **31**, 1385–1392 (2007)

Chakraborty, N., Klein, M., Swaminathan, N.: Effects of Lewis number on reactive scalar gradient alignment with local strain rate in turbulent premixed flames. Proc. Comb. Inst. **32**, 1409–1417 (2009)

Chakraborty, N., Hartung, G., Katragadda, M., Kaminski, C.F.: A numerical comparison of 2D and 3D density-weighted displacement speed statistics and implications for laser based measurements of flame displacement speed. Comb. Flame **158**, 1372–1390 (2011)

Chakraborty, N., Herbert, A., Ahmed, U., Im, H.G., Klein, M.: Assessment of extrapolation relations of displacement speed for detailed chemistry direct numerical simulation database of statistically planar turbulent premixed flames. Flow Turb. Comb. **108**, 489–507 (2022)

Chen, J., Im, H.G.: Correlation of flame speed with stretch in turbulent premixed methane/air flames. Proc. Comb. Inst. **27**, 819–826 (1998)

Dave, H., Chaudhuri, S.: Evolution of local flame displacement speeds in turbulence. J. Fluid Mech. **884**, A46 (2020)

Dopazo, C., Cifuentes, L., Martin, J., Jimenez, C.: Strain rates normal to approaching isoscalar surfaces in a turbulent premixed flame. Comb. Flame **162**, 1729–1736 (2015)

Dopazo, C., Cifuentes, L., Alwazzan, D., Chakraborty, N.: Influence of the lewis number on effective strain rates in weakly turbulent premixed combustion. Comb. Sci. Tech. **190**, 591–614 (2018)

Echekki, T., Chen, J.H.: Analysis of the contribution of curvature to premixed flame propagation. Comb. Flame **118**, 303–311 (1999)

Han, I., Huh, K.H.: Roles of displacement speed on evolution of flame surface density for different turbulent intensities and Lewis numbers for turbulent premixed combustion. Comb. Flame **152**, 194–205 (2008)

Herbert, A., Ahmed, U., Chakraborty, N., Klein, M.: Applicability of extrapolation relations for curvature and stretch rate dependences of displacement speed for statistically planar turbulent premixed flames. Comb. Theor. Modell. **24**, 1021–1038 (2020)

Keil, F.B., Amzehnhoff, M., Ahmed, U., Chakraborty, N., Klein, M.: Comparison of flame propagation statistics extracted from DNS based on simple and detailed chemistry part 1: fundamental flame turbulence interaction. Energies **14**, 5548 (2021a)

Keil, F.B., Amzehnhoff, M., Ahmed, U., Chakraborty, N., Klein, M.: Comparison of flame propagation statistics extracted from DNS based on simple and detailed chemistry Part 2: Influence of choice of reaction progress variable. Energies **14**, 5695 (2021b)

Klein, M., Chakraborty, N., Jenkins, K.W., Cant, R.S.: Effects of initial radius on the propagation of premixed flame kernels in a turbulent environment. Phys. Fluids **18**, 055102 (2006)

Klein, M., Chakraborty, N., Ketterl, S.: A comparison of strategies for direct numerical simulation of turbulence chemistry interaction in generic planar turbulent premixed flames. Flow Turb. Comb. **199**, 955–971 (2017)

Nivarti, G.V., Cant, R.S.: Stretch rate and displacement speed correlations for increasingly turbulent flames. Flow Turb. Comb. **102**, 957–971 (2019)

Ozel-Erol, G., Klein, M., Chakraborty, N.: Lewis number effects on flame speed statistics in spherical turbulent premixed flames. Flow Turb. Comb. **106**, 1043–1063 (2021)

Peters, N.: Turbulent Combustion. Cambridge Monograph on Mechanics. Cambridge University Press, Cambridge (2000)

Peters, N., Terhoeven, P., Chen, J.H., Echekki, T.: Statistics of flame displacement speeds from computations of 2-D unsteady methane-air flames. Proc. Comb. Inst. **27**, 833–839 (1998)

Poinsot, T., Lele, S.K.: Boundary conditions for direct simulation of compressible viscous flows. J. Comp. Phys. **101**, 104–129 (1992)

Poinsot, T., Veynante, D.: Theoretical and numerical combustion. R.T. Edwards Inc., Philadelphia, USA (2001)

Rogallo, R. S.: Numerical experiments in homogeneous turbulence, NASA technical memorandum 81315, NASA Ames research center, California (1981)

Varma, A.R., Ahmed, U., Klein, M., Chakraborty, N.: Effects of turbulent length scale on the bending effect of turbulent burning velocity in premixed turbulent combustion. Comb. Flame **233**, 111569 (2021)

Wray, A. A.: Minimal storage time advancement schemes for spectral methods, unpublished report, NASA Ames Research Center, California (1990)

Yu, R., Nillson, T., Fureby, C., Lipatnikov, A.N.: Assessment of an evolution equation for the displacement speed of a constant-density reactive scalar field. J. Fluid Mech. **911**, A138 (2021a)

Yu, R., Nillson, T., Brethouwer, G., Chakraborty, N., Lipatnikov, A.: Assessment of an evolution equation for the displacement speed of a constant-density reactive scalar field. Flow Turb. Comb. **106**, 1091–1110 (2021b)

Publisher's Note Springer Nature remains neutral with regard to jurisdictional claims in published maps and institutional affiliations.